

**MACHINE LEARNING-BASE ENHANCEMENT OF REMOTE SENSING IMAGE  
USING HYBRID MODEL****Kishore Singh<sup>1\*</sup>**

MTech Student, Department of Electrical &amp; Electronic Engineering, BRCM CET (127028) Bahal Haryana (Corresponding Author)

**Ashanand<sup>2</sup>****Dr. Vivek Kumar<sup>3</sup>**

Assistant Prof. of Electrical Engineering Department of BRCM CET (127028) Bahal Haryana.

HOD and Professor Electrical Engineering Department of BRCM CET (127028) Bahal Haryana.

---

**ABSTRACT**

A machine learning algorithm to improve images from remote sensing. In order to preserve textures and reduce haze, it enhances denoising or removes noise while maintaining picture information. The quality and efficacy of optical (RSI) are significantly compromised when cloud layers are present. To be more precise, the created feature is constrained by the scene-constraint item to reduce the possibility of scene changes. Haze, Gauss Filter, Non-Local Mean is an enhanced hierarchical model. High spatial resolution images are needed for the research work. In proposed method remote sensing images are used for evaluation. These images are providing with steps like non local means filter, Gauss filter and Haze removal. The quality of remote sensing images gets improved using enhancement steps. The proposed method is compared with other state-of-the-art methods, the resulting in remote sensing images with high quality results. Compared with these methods, our proposed method outperformed average increments of PSNR 63.758, SSIM 0.999, MSE 0.067 (NWPU-RESISC25), PSNR 49.077 and SSIM 0.997 (UC MERCED), PSNR 37.518 and SSIM 0.967 (AID) and PSNR 38.151, SSIM 0.980, MSE 12.6964 (WHU-RS19) datasets.

**Keywords:**

Machine Learning, Remote sensing image, non-local means filter, Enhancement

---

**INTRODUCTION**

Massive-scale satellite sensors and different earth observation platforms rely heavily on remote sensing images, which are now readily available in massive quantities. Many remote sensing applications, including semantic segmentation, target recognition, and scene classification, have historically preferred high spatial resolution aerial images with rich textures and high-frequency information. Available remote sensing images often has a poor resolution, especially when it comes to common civilian uses. Remote sensing with low resolution (LR) images decrease the accuracy of later computer vision tasks, but the best way to achieve spatial resolution images from LR counterparts is to use MATLAB software to achieve super-resolution (SR), which can overcome hardware restrictions. Machine learning has advanced significantly in the super-resolution of images. However, the current machine learning SR approaches of remote sensing pictures are prone to lose texture features, leading to excessive smoothing, because of the ill-posed character of the underdetermined issue in satellite image super-resolution. The discriminator network incorporates spectral normalization to stabilize the training process, while content integrity is utilized to tackle unstable training and vanishing gradient. The suggested model incorporates scene-constraint data to lower the possibility of scene variance. use cascade structure to increase the resolution of remote sensing images, which can provide arbitrary high-quality, high-time SR images [1,2,3].

Great-quality remote sensing images are in great demand in the military, earth sciences, agricultural, and astronomy sectors. However, less-than-ideal environmental conditions dim the light and isolate the important components in distant sensing images. For better information representation and visual perception, low-light

enhancement techniques are necessary, as brightness is a crucial quality factor in remote sensing images. In order to prevent gradient diffusion and model optimization direction deviation, peak signal-to-noise ratio (PSNR) and structural similarity (SSIM) quotient are used. The main drawback of a non-local mean filter is that its effects are amplified if it has peaks, which can lead to saturation problems and an overly sharpened image. Results show that it provides state-of-the-art performance in picture improvement using a synthesized low-light image enhancement dataset. Additionally, we help with object recognition on the improved image, which is beneficial for images used in remote sensing. Utilizing the feature fusion module to enhance the perception of multilayer features and low-scale texture details, reducing redundant information, and enabling the interaction of each branch's feature vectors across channels [4,5,6].

Image denoising, which lowers unwanted noise in deteriorated images, is important for contemporary imaging systems and has garnered a lot of interest from academics and business. Denoising an image may be thought of as an inverse issue, where noisy data are used to estimate the underlying clean image. Implemented and developed are the speckle denoise capabilities of NLM and other NLM-reprojection techniques. Dynamic positron emission tomography (PET) image denoising has been achieved by the development of NLM with a spatiotemporal search window (NLM-ST). Numerous research has looked at the theoretical elements of the NLM filter. Studying the NLM qualities in relation to segmentation based on the graph's spectral properties—which show how similar the neighborhoods in the image are—is done. The traditional NLM filter from a fresh angle and, based on the theoretical analysis, suggest an enhanced filter known as the clustering-based NLM filter. A non-subsampled shear-let transform utilizing non-subsampled pyramid and non-subsampled shearing filters is combined to provide a unique denoising solution for MRI images. This technique is based on the advanced NLM method [7,8,9].

One of the intrinsic parameters of remote sensing image is speckle noise. A random deterministic interference pattern called speckle deteriorates an image's borders and tiny features. The identification of tiny, low-contrast lesions is made more difficult by this phenomenon. An efficient way to eliminate sudden noise is by using a nonlinear filter. It lessens speckle as well. The output pixel value of the area's center location is the median intensity in the chosen region as applied by this filter. Error on the mean (MSE). The variation across a limited region is inversely related to the smoothing degree of the Lee filter. When variation is considerable, often in the vicinity of the edge, smoothing is not applied.

Depending on dividing the local standard deviation by the local mean of the deteriorating image, the weights are calculated. Within the moving window, a weighted average value takes the place of the relevant pixel. When the variation inside the window rises, the weighting factors increase and decrease in relation to the distance from the pixel of interest [10,11,12].

When employing post-reconstruction techniques for noise reduction in PET imaging, considerable signal and quantitative bias are frequently lost. To improve the signal-to-noise ratio (SNR) in PET image, edge-preserving denoising techniques were presented. These techniques aim to deliver effective noise reduction with low quantitative bias. The non-local mean approach (NLM), one of the edge-preserving denoising strategies, has shown promising results for the goal of noise reduction while maintaining important PET signals or underlying structures. The NLM denoising technique's basic principle is to search for comparable patterns or textures in the non-local regions of the image, which can be located any distance from the target voxel or patch. These types of redundant information are what NLM filters use to successfully separate the real signal from the undesired noise. These auxiliary images are made up of the target image's underlying structures and textures that have been tainted with various patterns or noise levels. As a result, these images make it possible to provide the NLM technique with extremely comparable (perfect) patches so that the target image may undergo denoising [13,14,15].

The amount of satellite images has significantly increased in recent years due to advancements in remote sensing technologies. High resolution images are advantageous for many remote sensing applications because they better reflect ground characteristics. Regrettably, throughout the data collection phase, meteorological conditions have an impact on remote sensing images. Haze often impairs satellite images, making the scene less visible and obscuring clarity, thereby lowering the quality of the image. Nonetheless, there is still a chance for ground surface radiance recovery because the ground feature may still be recognized. Haze-polluted visible images lose color purity and contrast, which has a negative impact on how humans understand and use them. Moreover, the reduced scene brightness will unavoidably impair the efficiency of several image processing methods. Haze reduction enhances the usability of the viewable images while also restoring their excellent

quality. In applications involving distant sensing images, it is greatly sought. Since images in hazy regions contain both earth surface characteristics and haze information, haze reduction for visible remote sensing images is a difficult problem. The problem is often hard to answer with a single haze image because the ground radiation is combined with hazy scattering light. Certain single-image dehazing methods are effective in handling blurry outside images. These techniques haven't been demonstrated to work well for remote sensing images, though. The approaches based on image enhancement make certain assumptions in order to extract distinct scenes from blurry images. On the premise that the histograms of clear and hazy regions are same, Richter suggested a histogram matching technique. It is believed that the low-frequency regions of the image include haze effects. The data in this section is replaced with a reference image that is devoid of haze using wavelet transform fusion. The same premise applies to approaches based on homomorphic filters. For high quality images, the assumptions made by these approaches could not hold true. Furthermore, it is certain that the global operations would cause the clear areas of the hazy image to become distorted [16,17,18,19,20].

Malaysian remote sensing data frequently has haze issues, especially in data collected at the end of the year. Large-scale forest fires from neighboring nations are linked to haze occurrences in Malaysia because of forest clearance efforts. Because the components of haze are mostly dependent on the wavelength of solar radiation, haze is produced by air scattering and absorption of solar light. Short wavelengths often experience substantially higher scattering than long wavelengths, which has a substantial impact on how surface features are classified from remote sensing data. This work aims to provide a workable haze reduction method so that the fuzzy data may be used once more. When it comes to haze reduction, it has to be accessible at all times and un-reliant on supplementary data like meteorological and haze path radiance. To calculate the haze path radiance, it is assumed that there are some completely black pixels (dark objects) in the image; these are often the result of cloud shadows or terrain. Since a dark object is thought to be incapable of reflecting any solar light, it should have reflectance or DN (digital number). These pixels seem partially dark if there is haze because the haze scatters solar radiation into the satellite's field of vision. An abrupt rise in the frequency of occurrence in the lower DN area may be observed in this effect by examining the histogram of a certain visible band. It is considered that the DN number corresponding to this rise represents the level of haze in that specific band. Although haze may also be indicated by smaller occurring DNs, this needs to be eliminated from the full image in order for that band to be responsible for the haze. Though straightforward and helpful in most cases, the haze value selected from the histogram might not match a true dark object because secondary energy scattered from other objects into the shadowed area could cause the shadow pixels caused by topography and clouds to have zero DN instead of zero. This may result in an excessive decrease of haze, which would truncate the results for some surface pixels. Therefore, this approach is not given any further thought. a method of reducing haze in a Landsat dataset that considers nonuniform haze by combining radiative transfer equation with image-based techniques. First, the less haze-affected near-infrared wavelengths.

We provide a machine learning-based approach for super-resolution of remote sensing images, incorporating content integrity and scene constraints, to address the previously described issues. To be precise, a machine learning framework is suggested in order to produce arbitrary high-quality, high-time SR remote sensing images. Next, scene information is included to limit the creation of details, hence preventing scene variation and lowering the likelihood of incorrect feature production. Next, scene information is included to restrict detail augmentation, preventing scene variation and lowering the possibility of mistakenly boosted features. Comprehensive test outcomes demonstrate that, both subjectively and objectively, our suggested machine learning approach outperforms current machine learning-based techniques. The remaining sections of this research are structured as follows: a succinct overview of relevant works on super-resolution satellite images; an in-depth analysis of the proposed method's experimental findings; and ablation studies. Lastly, we offer the debate and analysis [ 21,22,23,24].

### OBJECTIVES

The main objective of the study is to perform enhancement of remote sensing images. Enhancement in remote sensing images is essential for deriving valuable information for a range of uses. We can increase the data's readability and clarity by enhancing images using methods like sharpening, contrast modification, or noise removal. This is especially important in domains where decision-making requires exact information. Enhanced images help in identification of type and category of images.

**METHODOLOGY**

Our proposed method is hybrid model for remote sensing image enhancement. We Applied filter in our model are Non-Local Mean, Gaussian, Reduce Atmosphere Haze for better enhanced remote sensing image shown in Figure 1 and used datasets are WHU-RS19, NWPU-RESISC45, UC-MERCED, AID performed in MATLAB2018a.

The functioning of the proposed methodology for remote sensing image enhancement is expressed in figure 1. The description of the steps is illustrated as follows:

*Input Image:*

*Non local means filter:* The non local means filter is a non-linear, edge-preserving smoothing filter, in. The image block can be subjected to the filter, which modifies its pixels as the weighted sum of its neighboring pixels. The weighted parameter of the filter is established by the degree of similarity between the image block neighborhoods [35,36]. In proposed method when we applied non-local mean filter on green channel of remote sensing images from WHU-RS19, AID, NWPU-RESISC, UC-MERCED datasets. we observed noise got removed to get improved image with better visibility as compared to input remote sensing image.

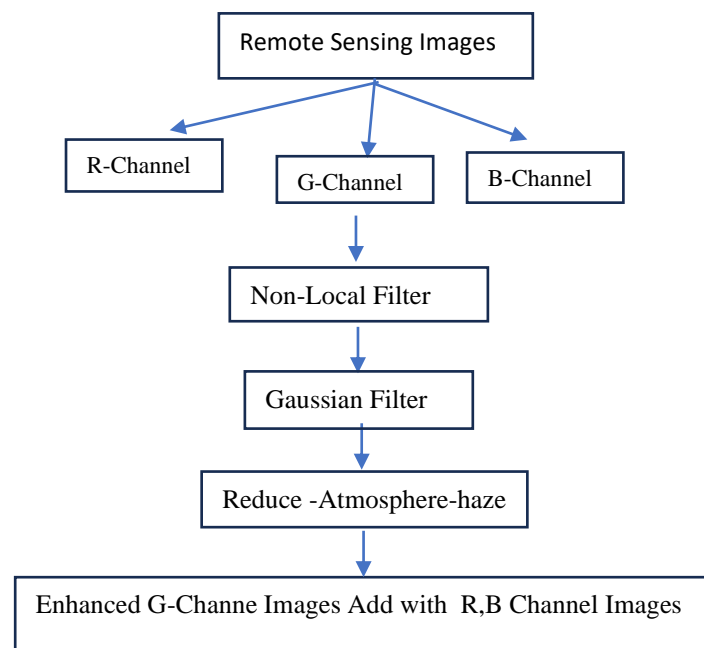


Figure 1 Enhancement model of remote sensing

*Gaussian filter:* When we applied gaussian filter on improved image which got from non-local mean filter, the gaussian noise get removed. The gaussian filter works by smoothing the image, reducing the high frequency component associated with noise thus making appear cleaner and more visually pleasing. We observed improved image 2-D qualitatively, edge detection, blur denoised and smoothing in image. The mean filter is one smoothing filter that reduces the weights of the kernel farther from the center, thus while it smooths out noise, it tends to keep the edges better. Image blending, which is used when seamless image transitions are needed. Radially symmetric, meaning it smooths equally in all directions, which avoids directional biases. One 1D Gaussian filter applied horizontally and one applied vertically can be separated from a 2D Gaussian filter. [37,38].

*Reduce Atmosphere Haze:* When we applied dehazing filter in image which passed through non-local mean filter and gaussian filter so we observed reduce atmosphere pollution, fog, reduce the clarity, visibility of image, improve the contrast and objects in image become sharper. The algorithm is based on a distorted haze imaging model and the dark channel prior [39,40].

### RESULTS AND DISCUSSION

It has been shown that texture structure and visual perception are connected to PSNR, MSE, ENTROPY, and SSIM. It may be demonstrated that CTF is not always superior than machine learning-based techniques. When compared WHU-RS19 in graph7 and NWPU-RESISC45 datasets in graph 8 to CGAN , SNSRGAN , EEGAN , SRGAN , LapSRN ,and UCMERCED datasets to DWT-SVD , BIMEF , CLAHE , DHE , SSR in graph 9 and AID datasets to BICUBIC , VDSR , LGCNET , PAN, DRSEN in graph 10 haze, and machine learning, which have similar performance in visual perception in texture structure, SR results by non-local mean, gaussian filter, and haze reduce suffer some decrease in both visual perception and texture structure because they improve edge, which helps to maintain texture structure. Haze removal is competitive when compared to all other comparing approaches, including non-local methods, because of its cascade structure, edge augmentation, and auxiliary label information. As given in table 1, table 2, table 3 and table 4, the comparison to alternative super resolution techniques, the hybrid model yields an average increase of 63.758 and SSIM 0.999 for NWPU-RESISC, 49.077 and 0.997 for UCMERCED, 38.1514 and 0.980 for WHU-RS19, and 37.158 and 0.967 for AID. We also do arbitrary high-time super-resolution in addition to these low-time picture super-resolutions, and the results show that our suggested hybrid model, particularly in high-time super-resolution, gets the highest average evaluations. It is also important to note that, in contrast to others, our technique delivers extremely steady performance even at large time scale factors, proving its ability to produce better SR outcomes in arbitrary time super-resolution. The last section's qualitative and quantitative results show that, in comparison to alternative methods, our HYBRID MODEL produces more agreeable SR outcomes. Nevertheless, since the ML divergence is used to maximize the objective function and regularizations are not used to stabilize the discriminator training in the HYBRID MODEL, there may be an unstable training issue. We have performed assessments on the super-resolution network's generative performance, which indicates its capacity to match the manifold of high-resolution images. We ask three experts in the field of remote sensing image interpretation to analysis sets of images subjectively and qualitatively. The WHU-RS19, AID, NWPU-RESISC45, and UCMERCED datasets scene categories are used to randomly choose the remote sensing images.

Table 1 Enhancement of UC MERCED datasets with metrics values

Object	PSNR	SSIM	ENTROPY	MSE
Agriculture	48.943	0.998	6.35	1.101
Airplane	49.533	0.998	6.975	0.775
Baseball Diamond	51.107	0.998	6.76	0.555
Beach	52.11	0.998	6.714	0.414
Building	48.679	0.998	7.365	1.200
Chaparral	48.679	0.998	7.365	1.200
Dense Residential	49.036	0.998	7.492	0.880
Forest	49.430	0.998	6.430	0.870

Freeway	49.625	0.998	7.095	0.814
Golf course	51.030	0.998	6.463	0.563
Harbor	47.442	0.998	7.062	1.40
Intersection	49.335	0.998	7.20	0.922
Medium Residential	48.055	0.998	7.369	1.100
Mobile home park	47.012	0.998	7.475	2.259
overpass	48.151	0.997	6.986	1.132
Parking lot	45.955	0.998	7.082	2.043
River	48.939	0.997	6.684	1.106
Runway	49.416	0.998	6.819	0.839
Spare Residential	49.163	0.998	7.053	0.904
Storage Tank	48.737	0.998	7.086	1.212
Tennis Court	50.248	0.998	7.078	0.703
Average	49.077	0.997	6.995	1.047

Table 2 Enhancement of AID datasets with metrics values

Object	PSNR	SSIM	ENTROPY	MSE
Airport	35.699	0.953	7.092	19.250
Bare land	39.737	0.981	6.498	8.363
Base ballfield	38.252	0.977	7.014	11.203
Beach	38.136	0.972	7.132	14.149
Bridge	37.120	0.959	6.593	15.939
Centre	34.830	0.950	7.433	25.765
Church	41.352	0.984	7.411	9.054
Commercial	35.682	0.959	7.225	19.660
Dense Residential	35.071	0.961	7.346	27.585
Desert	40.781	0.992	6.422	6.323
Farmland	40.261	0.974	6.393	8.980

Forest	36.298	0.964	6.483	19.364
Industrial	35.515	0.963	7.363	20.948
Meadow	36.527	0.953	6.069	18.157
Average	37.518	0.967	6.891	16.052

Table 3 Enhancement of NWPU-RESISC45 datasets with metrics values

Object	PSNR	SSIM	ENTROPY	MSE
Airplane	59.60	0.999	6.729	0.105
Airport	65.33	0.999	6.921	0.029
Baseball diamond	66.89	0.999	6.784	0.02
Basket ball court	61.70	0.999	6.920	0.068
Beach	61.97	0.999	7.114	0.059
Bridge	65.28	0.999	6.418	0.033
Chaparral	63.80	0.999	6.949	0.047
Church	60.182	0.999	7.291	0.110
Circular farmland	66.89	0.999	6.865	0.018
Cloud	65.67	0.999	7.168	0.026
Commercial area	62.43	0.999	7.169	0.060
Dense residential	61.29	0.999	7.259	0.092
Desert	64.178	0.999	6.706	0.048
Forest	66.68	0.999	6.365	0.036
Freeway	65.188	0.999	6.864	0.034
Golf course	68.51	0.999	6.50	0.014
Ground track field	65.931	0.999	6.989	0.025
Harbor	57.122	0.999	6.877	0.244
Industrial area	64.846	0.999	7.237	0.055
Intersection	69.529	0.999	7.238	0.117
Island	63.269	0.999	6.462	0.049
Lake	65.932	0.999	6.692	0.031

Meadow	68.456	0.999	5.996	0.0176
Medium residential	63.08	0.999	7.099	0.0531
Mobile home park	59.030	0.999	7.353	0.130
Mountain	68.297	0.999	6.81	0.014
Overpass	63.72	0.999	7.03	0.046
Palace	62.197	0.999	7.262	0.081
Parking lot	59.195	0.999	7.029	0.298
Railway	65.137	0.999	6.921	0.057
Railway station	63.330	0.999	7.044	0.044
Rectangular farmland	63.330	0.999	7.044	0.044
River	67.57	0.999	6.756	0.017
Round about	63.06	0.999	7.133	0.05
Runway	62.77	0.999	6.480	0.054
Sea ice	63.45	0.999	6.465	0.052
Ship	62.05	0.999	6.384	0.067
Snow berg	56.06	0.999	7.421	0.344
Spare residential	63.41	0.999	6.76	0.044
Stadium	62.581	0.999	7.243	0.060
Storage tank	60.44	0.999	7.280	0.082
Tennis court	63.86	0.999	7.040	0.040
Terrace	66.918	0.999	6.602	0.019
Thermal power station	62.119	0.999	7.119	0.067
wetland	66.84	0.999	6.338	0.022
Average	63.758	0.999	6.891	0.067

Table 4 Enhancement of WHU-RS19 datasets with metrics value

Object	PSNR	SSIM	ENTROPY	MSE
Airport	37.307	0.993	5.621	2.156



Beach	45.5323	0.993	5.621	2.156
Bridge	41.548	0.985	6.263	5.2199
Commercial	35.297	0.971	7.574	19.693
Desert	42.568	0.9968	6.683	3.946
Farmland	41.595	0.981	6.028	4.887
Foot-ballfield	37.881	0.9797	7.574	11.278
Forest	36.778	0.978	6.723	15.127
industrial	36.611	0.976	7.501	14.916
meadow	41.768	0.990	6.1075	9.496
mountain	33.281	0.9669	7.161	32.34
park	36.601	0.968	7.04	16.03
parking	37.911	0.980	7.246	11.184
pond	39.402	0.985	6.692	8.041
port	37.485	0.982	7.119	12.308
Railway station	35.133	0.970	7.261	21.673
Residential	35.580	0.975	7.709	18.594
River	36.833	0.979	7.210	14.310
Viaduct	35.767	0.974	7.533	17.820
Average	38.1514	0.9801	6.8771	12.6964

The Graphical representation of comparison of results obtained for proposed method and other method is shown in

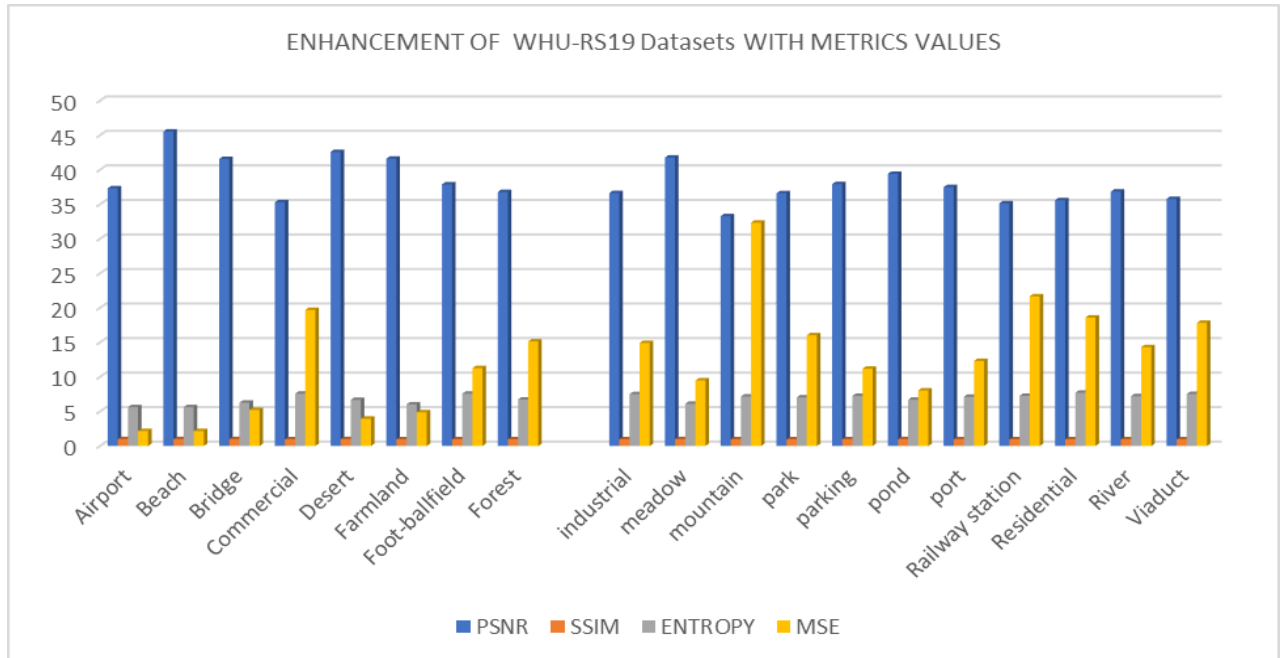


Figure 2 Graph of WHU-RS19 datasets with metrics values.

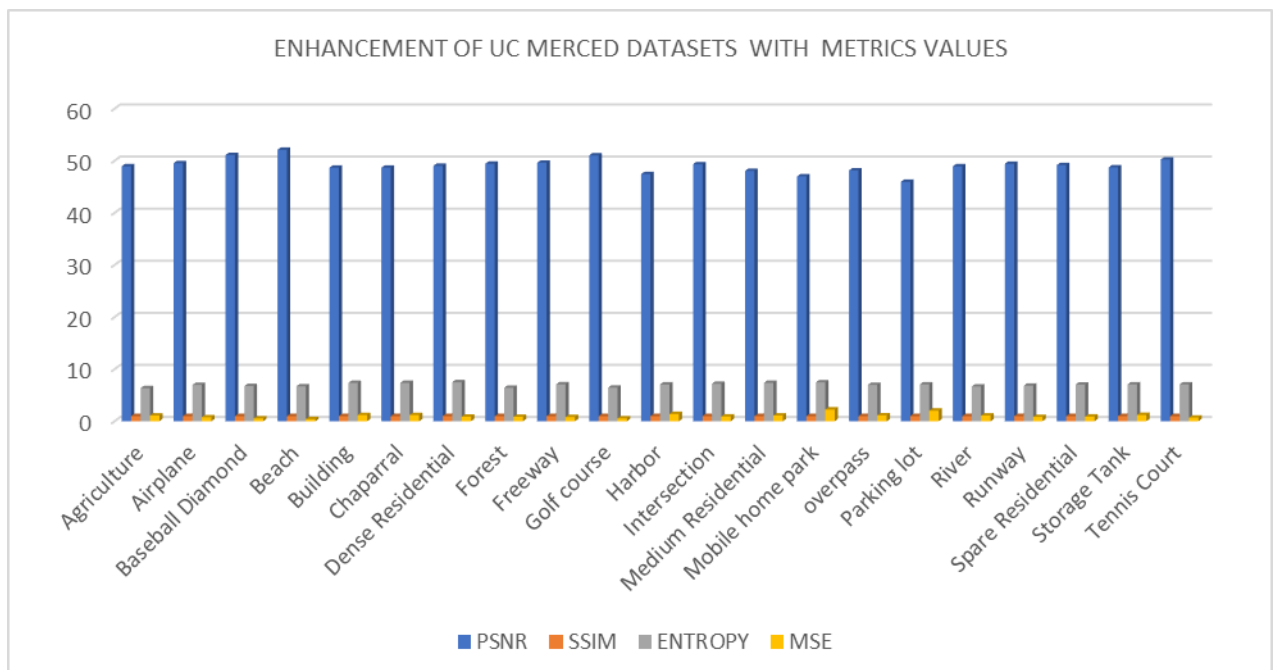


Figure 3 Graph of Enhancement of UC-Merced datasets with metrics values.

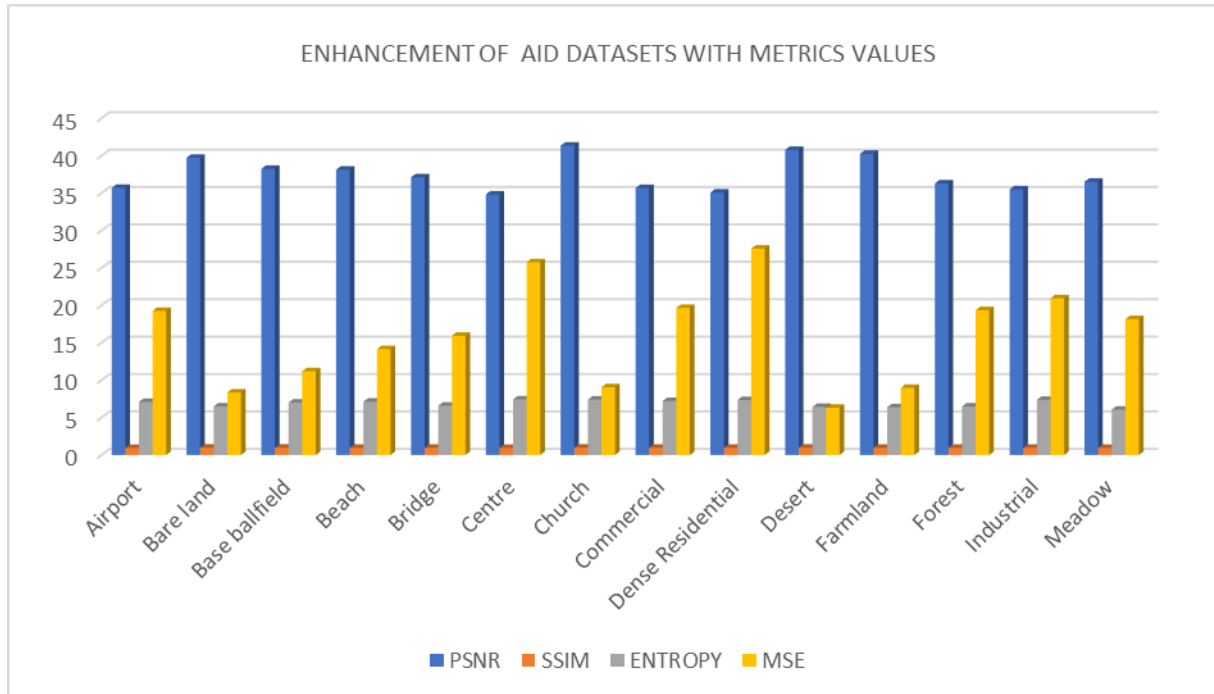


Figure 4 Graph of Enhancement of AID datasets with metrics values.

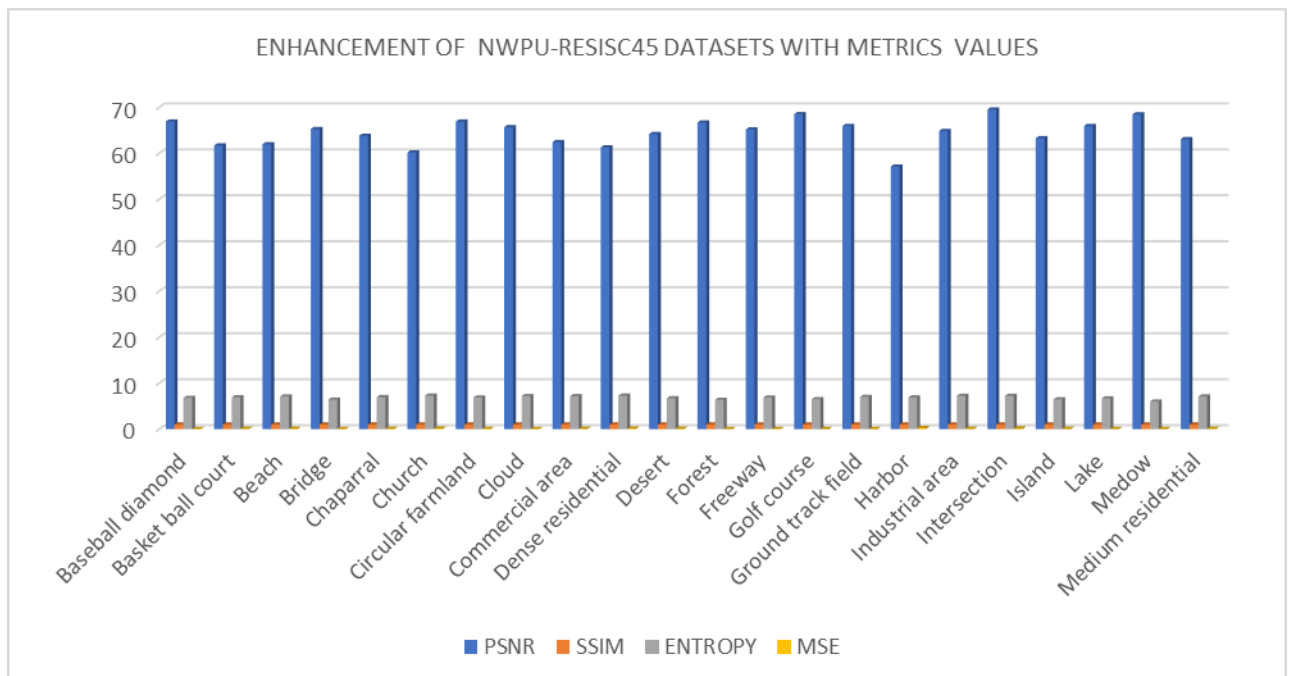


Figure 5 Graph of Enhancement of NWPU-RESISC45 datasets with metrics values.

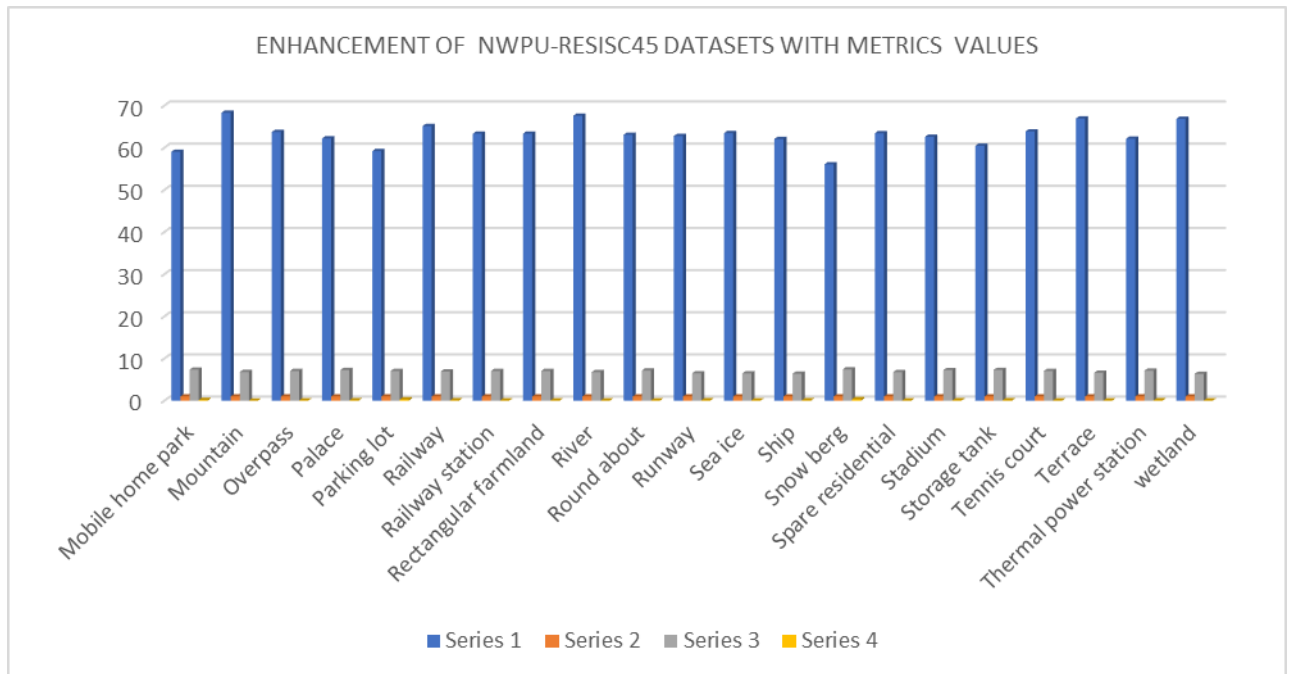


Figure 6 Graph of Enhancement of NWPU-RESISC45 with metrics values.

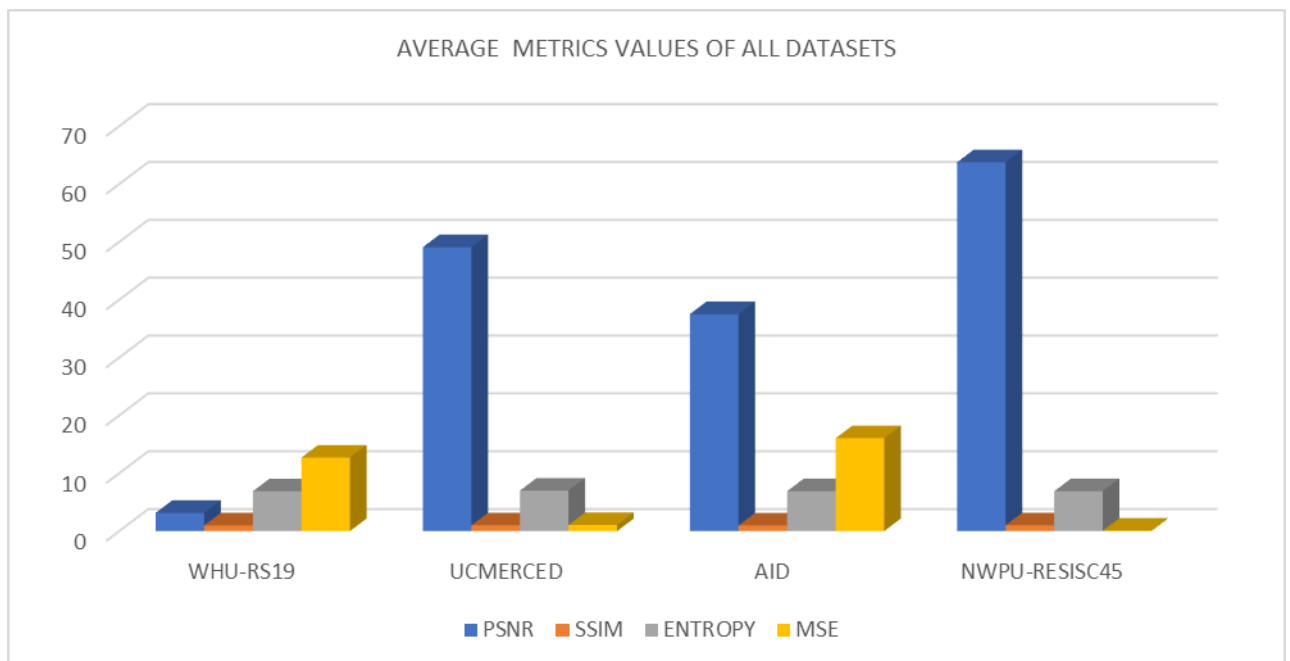














Figure 7 Graph of Average metrics values of all datasets.

In Figure 7 we shown average metrics value of all datasets are WHU-RS19, UC-MERCED, AID, NWPU-RESISC.

Table 6 Proposed method enhanced images comparison with different datasets original images.







DATASETS	OBJECTS	ORIGINAL IMAGE	ENHNACED IMAGE
WHU-RS19	BEACH ( Beach-01 )		 PSNR 45.532 SSIM 0.993 MSE 2.15
	DESERT ( Desert_01 )		 PSNR 42.568 SSIM 0.9968 MSE 3.946

NWPU-RESISC45	INTERSECTION (Intersection_001 )			PSNR 69.529 SSIM 0.999 MSE 0.117
	GOLF_COURSE (golf_course_001 )			PSNR 68.51 SSIM 0.999 MSE 0.014
AID	CHURCH ( Church_1 )			PSNR 41.352 SSIM 0.984 MSE9 9.054
	FARMLAND ( farmland_1 )			PSNR 40.261 SSIM 0.974

			MSE 8.980
UCMERCED	Baseball Diamond  (Baseball Diamond 01 )		  PSNR 51.107 SSIM 0.998 MSE 0.555
	TENNIS COURT  ( tenniscourt00 )		  PSNR 50.248 SSIM 0.998 MSE 0.703

In Table 6 we shown Proposed method enhanced images comparison with different datasets original images.

Table 7 Quantitatively objective comparison of WHU-RS19 datasets to different methods.

METHODS	PSNR	SSIM	MSE	IMAGES ( bridge )
CGAN [1]	27.15	0.948	0.041	 Bridge
SNSRGAN [49]	25.01	0.913	0.076	
EEGAN [50]	25.87	0.929	0.078	
SRGAN [48]	24.82	0.862	0.118	
LapSRN [51]	24.26	0.897	0.109	
PROPOSED METHOD	38.1514	0.9801	12.6964	



In Table 7 Quantitatively objective comparison of WHU-RS19 datasets to different methods.

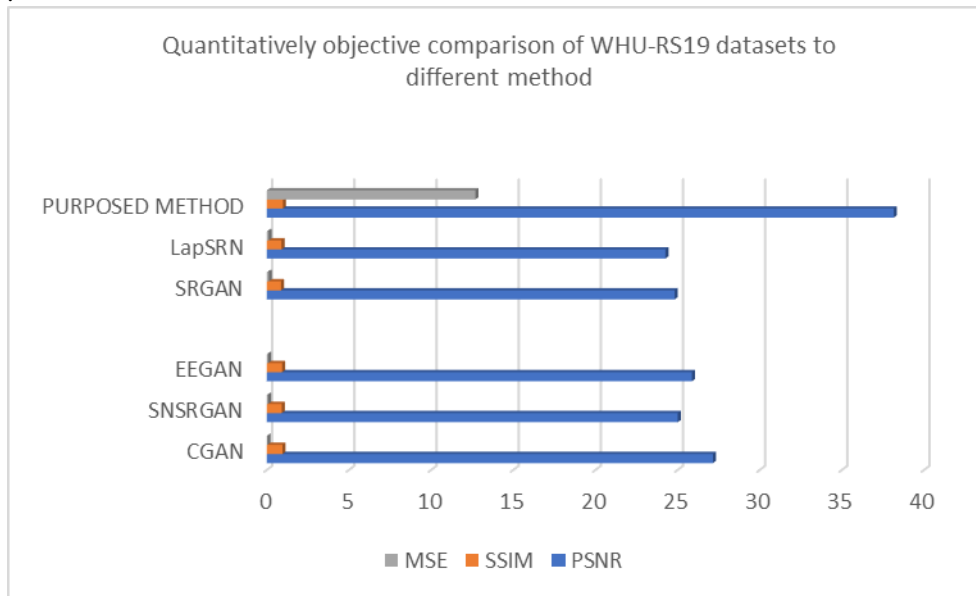





Figure 8 Graph of Quantitatively objective comparison of WHU-RS19 datasets to different methods.

Table 8 Quantitatively objective comparison of NWPU-RESISC45 datasets to different methods.

METHODS	PSNR	SSIM	MSE	IMAGES ( round about )
CGAN [1]	26.15	0.952	0.037	
SNSRGAN [41]	25.07	0.923	0.043	
EEGAN [42]	25.12	0.936	0.045	

SRGAN [43]	24.73	0.876	0.058	
LapSRN [44]	25.10	0.903	0.069	
PURPOSED METHOD	63.758	0.999	0.067	

In Table 8 Quantitatively objective comparison of NWPU-RESISC45 datasets to different methods.

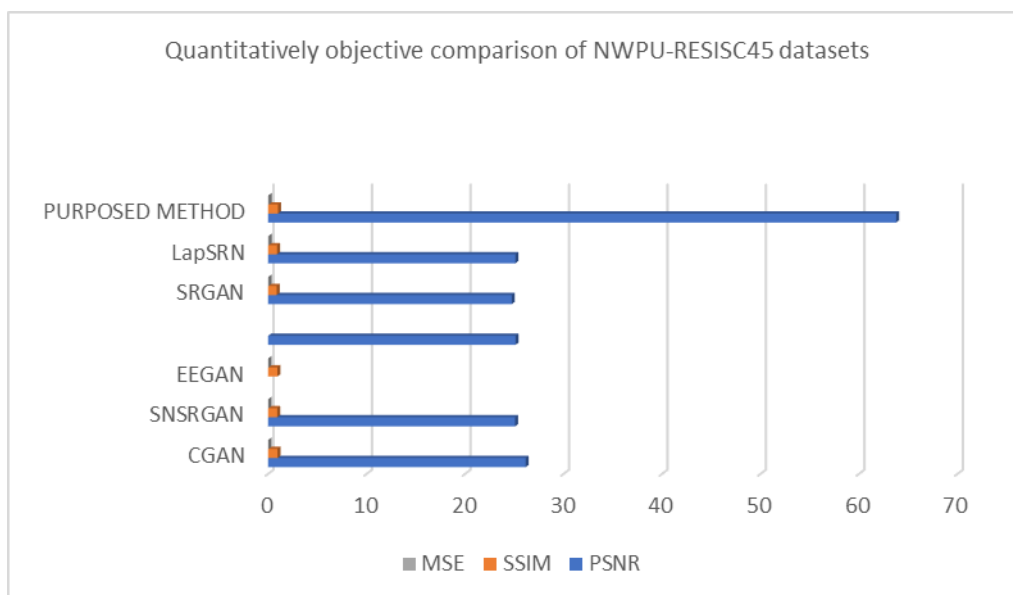








Figure 9 Graph of Quantitatively objective comparison of NWPU-RESISC45 datasets.

Table 9 Quantitatively objective comparison of UCMERGED datasets to different methods.

METHODS	PSNR	SSIM	IMAGE
DWT-SVD [45]	13.989	0.564	
BIMEF [46]	16.302	0.728	
CLAHE [47]	13.857	0.546	
DHE [48]	16.357	0.706	
SSR [49]	20.424	0.711	

PURPOSED METHOD	49.077	0.997	
-----------------	--------	-------	-------------------------------------------------------------------------------------

In Table 9 Quantitatively objective comparison of UCMERCED datasets to different methods.

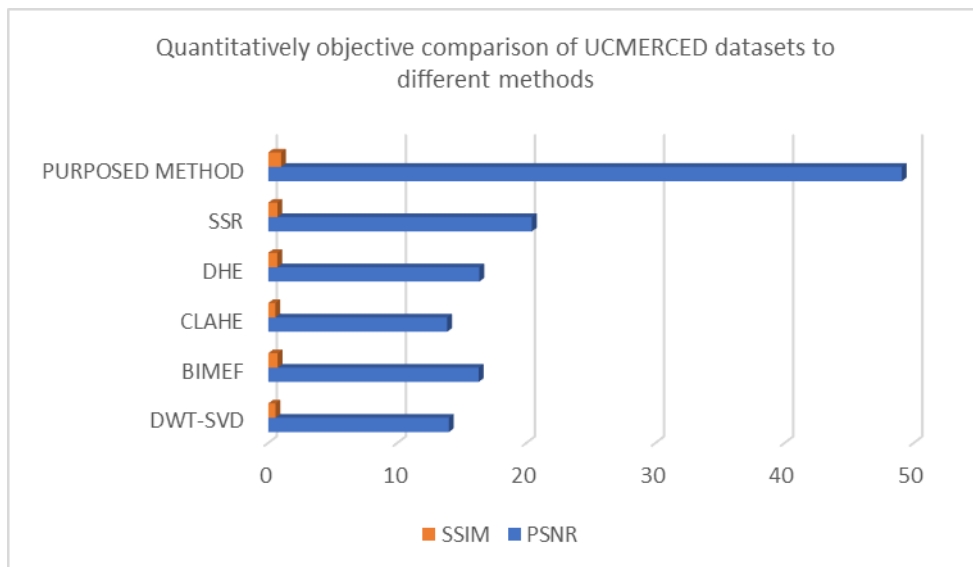
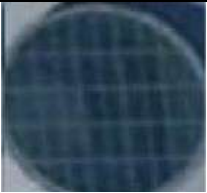



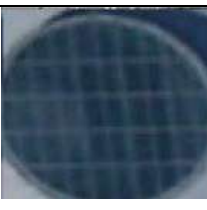



Figure 10 Graph of Quantitatively objective comparison of UCMERCED datasets to different methods.

Table 10 Quantitatively objective comparison of AID datasets to different methods.

METHODS	PSNR	SSIM	IMAGES
A+ [50]	29.14	0.8125	

SRCNN [51]	29.21	0.8118	
VDSR [52]	29.37	0.8128	
FSRCNN [53]	29.54	0.8139	
EDSR [54]	29.61	0.8153	
PURPOSED METHOD	37.518	0.967	

In Table 10 Quantitatively objective comparison of AID datasets to different methods.

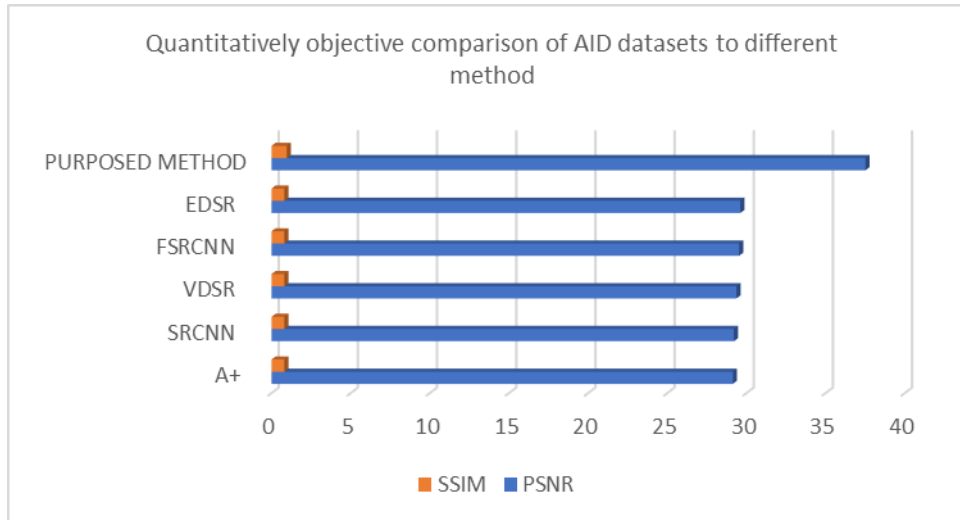


Figure 11 Graph of Quantitatively objective comparison of AID datasets to different methods.

### CONCLUSION

This paper suggests a method for remote sensing image enhancement that is based on Machine learning. In order to demonstrate the proposed method, Remote sensing image datasets are used like NWPU-RESISC25, UC MERCED, AID and WHU-RS19. Initially, in the first step non local means filter and gaussian filter are applied for removing the noise present in the image. The haze removal steps filters the haze from the image makes the image more clearer. The experimental findings demonstrate that, our proposed method outperformed average increments of PSNR 63.758, SSIM 0.999, MSE 0.067 (NWPU-RESISC25), PSNR 49.077 and SSIM 0.997 (UC MERCED), PSNR 37.518 and SSIM 0.967 (AID) and PSNR 38.151, SSIM 0.980, MSE 12.6964 (WHU-RS19) datasets. The results obtained outperformed the state-of-the-art methods.

### ACKNOWLEDGEMENT

We acknowledge the faculty members from Department of Electrical and Electronics Engineering of BRCM College of Engineering and Technology, Bahal, District Bhiwani, Haryana, India. Mr. Ashanand and Dr. Vivek Kumar who provided insight and expertise that greatly assisted the research. We are expressing our gratitude to our families for being an inspiration. Above all, to God.

### REFERENCES

- [1] Guo, D., Xia, Y., Xu, L., Li, W., & Luo, X. (2021). Remote sensing image super-resolution using cascade generative adversarial nets. *Neurocomputing*, 443, 117-130.
- [2] Odena, A., Olah, C., & Shlens, J. (2017, July). Conditional image synthesis with auxiliary classifier gans. In *International conference on machine learning* (pp. 2642-2651). PMLR.
- [3] Arjovsky, M., Chintala, S., & Bottou, L. (2017, July). Wasserstein generative adversarial networks. In *International conference on machine learning* (pp. 214-223). PMLR.
- [4] Zhao, M., Yang, R., Hu, M., & Liu, B. (2024). Deep Learning-Based Technique for Remote Sensing Image Enhancement Using Multiscale Feature Fusion. *Sensors*, 24(2), 673.
- [5] Cai, J., Gu, S., & Zhang, L. (2018). Learning a deep single image contrast enhancer from multi-exposure images. *IEEE Transactions on Image Processing*, 27(4), 2049-2062.

- [6] Demirel, H., Ozcinar, C., & Anbarjafari, G. (2009). Satellite image contrast enhancement using discrete wavelet transform and singular value decomposition. *IEEE Geoscience and remote sensing letters*, 7(2), 333-337.
- [7] Liu, X., Wu, Z., & Wang, X. (2023). The validity analysis of the non-local mean filter and a derived novel denoising method. *Virtual Reality & Intelligent Hardware*, 5(4), 338-350.
- [8] Sharma, A., & Chaurasia, V. (2021). MRI denoising using advanced NLM filtering with non-subsampled shearlet transform. *Signal, Image and Video Processing*, 15, 1331-1339.
- [9] Liu, G., Zhong, H., & Jiao, L. (2015). Comparing noisy patches for image denoising: A double noise similarity model. *IEEE Transactions on Image Processing*, 24(3), 862-872.
- [10] Xu, B., Cui, Y., Li, Z., & Yang, J. (2015). An iterative SAR image filtering method using nonlocal sparse model. *IEEE geoscience and remote sensing letters*, 12(8), 1635-1639.
- [11] Geng, J., Fan, J., Ma, X., Wang, H., & Cao, K. (2016, July). An iterative low-rank representation for SAR image despeckling. In *2016 IEEE International Geoscience and Remote Sensing Symposium (IGARSS)* (pp. 72-75). IEEE.
- [12] Lee, J. S. (1980). Digital image enhancement and noise filtering by use of local statistics. *IEEE transactions on pattern analysis and machine intelligence*, (2), 165-168.
- [13] Arabi, H., & Zaidi, H. (2020). Applications of artificial intelligence and deep learning in molecular imaging and radiotherapy. *European Journal of Hybrid Imaging*, 4, 1-23.
- [14] Hong, X., Zan, Y., Weng, F., Tao, W., Peng, Q., & Huang, Q. (2018). Enhancing the image quality via transferred deep residual learning of coarse PET sinograms. *IEEE transactions on medical imaging*, 37(10), 2322-2332.
- [15] Gong, K., Berg, E., Cherry, S. R., & Qi, J. (2019). Machine learning in PET: from photon detection to quantitative image reconstruction. *Proceedings of the IEEE*, 108(1), 51-68.
- [16] Liu, Q., Gao, X., He, L., & Lu, W. (2017). Haze removal for a single visible remote sensing image. *Signal Processing*, 137, 33-43.
- [17] Rudin, L. I., Osher, S., & Fatemi, E. (1992). Nonlinear total variation based noise removal algorithms. *Physica D: nonlinear phenomena*, 60(1-4), 259-268.
- [18] Richter, R. (1996). Atmospheric correction of satellite data with haze removal including a haze/clear transition region. *Computers & Geosciences*, 22(6), 675-681.
- [19] Liu, C., Hu, J., Lin, Y., Wu, S., & Huang, W. (2011). Haze detection, perfection and removal for high spatial resolution satellite imagery. *International Journal of Remote Sensing*, 32(23), 8685-8697.
- [20] Moro, G. D., & Halounova, L. (2007). Haze removal for high-resolution satellite data: a case study. *International Journal of Remote Sensing*, 28(10), 2187-2205.
- [21] Ahmad, A., Ghani, M. K. A., Razali, S., Sakidin, H., & Hashim, N. M. (2014). Haze reduction from remotely sensed data. *Applied Mathematical Sciences*, 8(36), 1755-1762.
- [22] Ahmad, A., & Hashim, M. (2002). Determination of haze using NOAA-14 AVHRR satellite data. *MACRES bulletin*, 15-27.
- [23] Schott, J. R., Salvaggio, C., & Volchok, W. J. (1988). Radiometric scene normalization using pseudoinvariant features. *Remote sensing of Environment*, 26(1), 1-16.
- [24] Chavez Jr, P. S. (1988). An improved dark-object subtraction technique for atmospheric scattering correction of multispectral data. *Remote sensing of environment*, 24(3), 459-479.
- [25] Guo, D., Xia, Y., Xu, L., Li, W., & Luo, X. (2021). Remote sensing image super-resolution using cascade generative adversarial nets. *Neurocomputing*, 443, 117-130.
- [26] Lim, B., Son, S., Kim, H., Nah, S., & Mu Lee, K. (2017). Enhanced deep residual networks for single image super-resolution. In *Proceedings of the IEEE conference on computer vision and pattern recognition workshops* (pp. 136-144).
- [27] Jiang, K., Wang, Z., Yi, P., Wang, G., Lu, T., & Jiang, J. (2019). Edge-enhanced GAN for remote sensing image superresolution. *IEEE Transactions on Geoscience and Remote Sensing*, 57(8), 5799-5812.
- [28] Dong, W., Wang, C., Sun, H., Teng, Y., Liu, H., Zhang, Y., ... & Xu, X. (2024). End-to-End Detail-Enhanced Dehazing Network for Remote Sensing Images. *Remote Sensing*, 16(2), 225.
- [29] Wang, T., Zhao, L., Huang, P., Zhang, X., & Xu, J. (2021). Haze concentration adaptive network for image dehazing. *Neurocomputing*, 439, 75-85.

- [30] Cai, B., Xu, X., Jia, K., Qing, C., & Tao, D. (2016). Dehazenet: An end-to-end system for single image haze removal. *IEEE transactions on image processing*, 25(11), 5187-5198.
- [31] Sui, J., Ma, Y., Yang, W., Zhang, X., Pun, M. O., & Liu, J. (2024). Diffusion Enhancement for Cloud Removal in Ultra-Resolution Remote Sensing Imagery. *arXiv preprint arXiv:2401.15105*.
- [32] Zhou, D., Yang, Z., & Yang, Y. (2023). Pyramid Diffusion Models For Low-light Image Enhancement. *arXiv preprint arXiv:2305.10028*.
- [33] Jing, R., Duan, F., Lu, F., Zhang, M., & Zhao, W. (2023). Denoising Diffusion Probabilistic Feature-Based Network for Cloud Removal in Sentinel-2 Imagery. *Remote Sensing*, 15(9), 2217.
- [34] Pan, H. (2020). Cloud removal for remote sensing imagery via spatial attention generative adversarial network. *arXiv preprint arXiv:2009.13015*.
- [35] Wang, C., Zhou, J., & Liu, S. (2013). Adaptive non-local means filter for image deblurring. *Signal Processing: Image Communication*, 28(5), 522-530.
- [36] I.H. Jang, N.C. Kim, H.J So, Iterative blocking artifact reduction using a minimum mean square error filters in wavelet domain. *Signal Processing* 83 (12) (2003) 2607–2619.
- [37] Deng, G., & Cahill, L. W. (1993, October). An adaptive Gaussian filter for noise reduction and edge detection. In *1993 IEEE conference record nuclear science symposium and medical imaging conference* (pp. 1615-1619). IEEE.
- [38] Hodson, E., Thayer, D., & Franklin, C. (1981). Adaptive Gaussian filtering and local frequency estimates using local curvature analysis. *IEEE Transactions on Acoustics, Speech, and Signal Processing*, 29(4), 854-859.
- [39] Pan, X., Xie, F., Jiang, Z., & Yin, J. (2015). Haze removal for a single remote sensing image based on deformed haze imaging model. *IEEE Signal Processing Letters*, 22(10), 1806-1810.
- [40] Long, J., Shi, Z., Tang, W., & Zhang, C. (2013). Single remote sensing image dehazing. *IEEE Geoscience and Remote Sensing Letters*, 11(1), 59-63.
- [41] Xu, L., Zeng, X., Huang, Z., Li, W., & Zhang, H. (2020). Low-dose chest X-ray image super-resolution using generative adversarial nets with spectral normalization. *Biomedical Signal Processing and Control*, 55, 101600.
- [42] Jiang, K., Wang, Z., Yi, P., Wang, G., Lu, T., & Jiang, J. (2019). Edge-enhanced GAN for remote sensing image superresolution. *IEEE Transactions on Geoscience and Remote Sensing*, 57(8), 5799-5812.
- [43] Ledig, C., Theis, L., Huszár, F., Caballero, J., Cunningham, A., Acosta, A., ... & Shi, W. (2017). Photo-realistic single image super-resolution using a generative adversarial network. In *Proceedings of the IEEE conference on computer vision and pattern recognition* (pp. 4681-4690).
- [44] Lai, W. S., Huang, J. B., Ahuja, N., & Yang, M. H. (2017). Deep laplacian pyramid networks for fast and accurate super-resolution. In *Proceedings of the IEEE conference on computer vision and pattern recognition* (pp. 624-632).
- [45] Demirel, H., Ozcinar, C., & Anbarjafari, G. (2009). Satellite image contrast enhancement using discrete wavelet transform and singular value decomposition. *IEEE Geoscience and remote sensing letters*, 7(2), 333-337.
- [46] Ying, Z., Li, G., & Gao, W. (2017). A bio-inspired multi-exposure fusion framework for low-light image enhancement. *arXiv preprint arXiv:1711.00591*.
- [47] Asha, S., & Sreenivasulu, G. (2018). Satellite image enhancement using contrast limited adaptive histogram equalization. *Int. J. Sci. Res. Sci. Eng. Technol*, 4(1), 1070-1075.
- [48] Abdullah-Al-Wadud, M., Kabir, M. H., Dewan, M. A. A., & Chae, O. (2007). A dynamic histogram equalization for image contrast enhancement. *IEEE transactions on consumer electronics*, 53(2), 593-600.
- [49] Jobson, D. J., Rahman, Z. U., & Woodell, G. A. (1997). Properties and performance of a center/surround retinex. *IEEE transactions on image processing*, 6(3), 451-462.



# IJETRM

## International Journal of Engineering Technology Research & Management

Published By:

<https://www.ijetrm.com/>

- [50] Timofte, R., De Smet, V., & Van Gool, L. (2015). A+: Adjusted anchored neighborhood regression for fast super-resolution. In *Computer Vision--ACCV 2014: 12th Asian Conference on Computer Vision, Singapore, Singapore, November 1-5, 2014, Revised Selected Papers, Part IV 12* (pp. 111-126). Springer International Publishing.
- [51] Dong, C., Loy, C. C., He, K., & Tang, X. (2014). Learning a deep convolutional network for image super-resolution. In *Computer Vision--ECCV 2014: 13th European Conference, Zurich, Switzerland, September 6-12, 2014, Proceedings, Part IV 13* (pp. 184-199). Springer International Publishing.
- [52] Kim, J., Lee, J. K., & Lee, K. M. (2016). Accurate image super-resolution using very deep convolutional networks. In *Proceedings of the IEEE conference on computer vision and pattern recognition* (pp. 1646-1654).
- [53] Dong, C., Loy, C. C., & Tang, X. (2016). Accelerating the super-resolution convolutional neural network. In *Computer Vision--ECCV 2016: 14th European Conference, Amsterdam, The Netherlands, October 11-14, 2016, Proceedings, Part II 14* (pp. 391-407). Springer International Publishing.
- [54] Lim, B., Son, S., Kim, H., Nah, S., & Mu Lee, K. (2017). Enhanced deep residual networks for single image super-resolution. In *Proceedings of the IEEE conference on computer vision and pattern recognition workshops* (pp. 136-144).